Water Research 252 (2024) 121236

Contents lists available at ScienceDirect

Water Research

journal homepage: www.elsevier.com/locate/watres

An integrated analytical modeling framework for determining site-specific soil screening levels for PFAS

Jacob Smith [a], Mark L. Brusseau [a,b], Bo Guo [a,*]

[a] Department of Hydrology and Atmospheric Sciences, University of Arizona, United States of America
[b] Department of Environmental Science, University of Arizona, United States of America

ARTICLE INFO

Keywords:
Per- and polyfluoroalkyl substances (PFAS)
Soil screening levels (SSLs)
Attenuation and dilution
Vadose zone
Groundwater
Maximum contaminant level (MCL)

ABSTRACT

Soils at many contaminated sites have accumulated a significant amount of per- and polyfluoroalkyl substances (PFAS) and may require remediation to mitigate leaching to groundwater. USEPA's current approaches for determining soil screening levels (SSLs) were developed for non-PFAS contaminants. Because many PFAS are interfacially-active with unique leaching behaviors in soils, the current non-PFAS-specific soil screening models may not be applicable. Following USEPA's general methodology, we develop a new modeling framework representing PFAS-specific transport processes for determining site-specific SSLs for PFAS-contaminated sites. We couple a process-based analytical model for PFAS leaching in the vadose zone and a dilution factor model for groundwater in an integrated framework. We apply the new modeling framework to two typical types of contaminated sites. Comparisons with the standard USEPA SSL approach suggest that accounting for the PFAS-specific transport processes may significantly increase the SSL for some PFAS. For the range of soil properties and groundwater recharge rates examined, while SSLs determined with the new model are less than a factor of 2 different from the standard-model values for less interfacially-active shorter-chain PFAS, they are up to two orders of magnitudes greater for more interfacially-active longer-chain PFAS. The new analytical modeling framework provides an effective tool for deriving more accurate site-specific SSLs and improving site characterization and remedial efforts at PFAS-contaminated sites.

1. Introduction

Per- and polyfluoroalkyl substances (PFAS) have been widely used since the 1940s for various applications, including fire-fighting, waterproofing and repellant materials, and food and industrial applications (Buck et al., 2011; ITRC, 2019). The wide applications over many decades have led to the ubiquitous presence of PFAS in the environment. In particular, PFAS have accumulated significantly in the vadose zone at many contaminated sites (Xiao et al., 2015; Weber et al., 2017; Dauchy et al., 2019; Høisæter et al., 2019; Anderson et al., 2019; Brusseau et al., 2020; Adamson et al., 2020; Cáñez et al., 2021; Quinnan et al., 2021; Anderson et al., 2022; Schaefer et al., 2022). Driven by infiltration events, PFAS migrate downward and pose significant risks to contaminate the groundwater underneath (e.g., Guo et al., 2020; Anderson, 2021; Schaefer et al., 2023).

Given that vadose zones at many PFAS-contaminated sites serve as long-term sources of PFAS to contaminate groundwater, remediation of the contaminated soils in the vadose zone may be required to protect the groundwater underneath. For this purpose, it is important to determine whether and to what extent a specific site requires further attention. Identifying contaminated sites of concern is commonly achieved by developing a site-specific soil screening level (SSL), which refers to the maximum concentration of a contaminant in the soil that is considered protective to human health along a specified pathway of exposure, such as groundwater resources (USEPA, 1996). In 1996, the United States Environmental Protection Agency (USEPA) developed an SSL framework to address these questions for traditional non-PFAS contaminants (USEPA, 1996). The USEPA SSL framework has been widely applied for determining SSLs for the migration of various contaminants to groundwater.

The development of SSLs often involves backward calculations starting from a given acceptable groundwater concentration, e.g., the maximum contaminant level (MCL) in groundwater. Multiple approaches of varying complexity have been developed for linking the MCL to SSLs. The simplest approach in the existing USEPA framework is to directly multiply an MCL by a dilution–attenuation factor (DAF) to determine a representative concentration of the contaminant of concern in porewater. In this simplest approach, the DAF accounts for dilution and attenuation in groundwater only, not in the vadose zone. This porewater concentration is then converted to an SSL assuming linear

* Corresponding author.
E-mail address: boguo@arizona.edu (B. Guo).

https://doi.org/10.1016/j.watres.2024.121236
Received 5 December 2023; Received in revised form 25 January 2024; Accepted 28 January 2024
Available online 1 February 2024

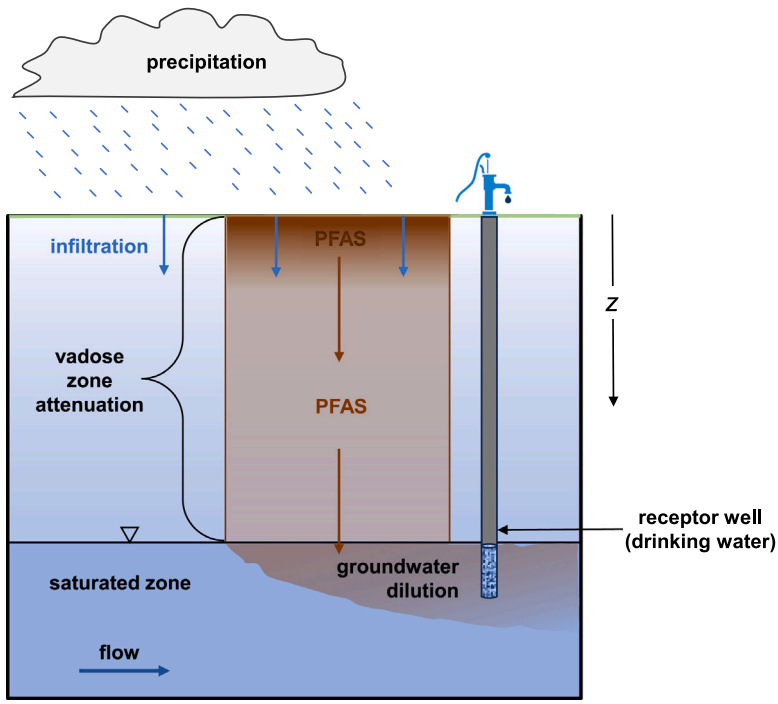

Fig. 1. A conceptual model for PFAS attenuation and dilution in the vadose zone and groundwater. PFAS released to the surface leach downward through the vadose zone to groundwater driven by water infiltration flux. A receptor well is assumed to be located at the edge of the source zone.

and equilibrium solid-phase adsorption and, if relevant, linear and equilibrium partitioning in the air phase. The more complex approaches frequently involve process-based models that represent the fate and transport of contaminants in both the vadose zone and groundwater, where attenuation and dilution can both occur. Often, a transport model for the vadose zone is combined with another model for groundwater. These transport models range from simple uniform mixing models (Connor et al., 1997) to analytical and to more complex numerical models (USEPA, 1996). These combined vadose-zone-groundwater modeling frameworks can be used to inversely derive SSLs given an MCL in groundwater. Additionally, they can also be used to determine contamination risks in groundwater based on current soil contamination conditions.

While many of these previous models have been widely used to derive site-specific SSLs, they may not be applicable to PFAS, which have unique interfacially-active properties. Many PFAS are surfactants and accumulate at the air–water interfaces in water-unsaturated soils (e.g., Brusseau, 2018; Lyu et al., 2018; Brusseau et al., 2019; Costanza et al., 2019; Silva et al., 2019; Schaefer et al., 2019a). Adsorption at air–water interfaces and potentially complex interactions with the solid (e.g., solid-phase adsorption) have been shown to significantly increase the retention of PFAS in the vadose zone (e.g., Guo et al., 2020; Silva et al., 2020; Zeng et al., 2021; Zeng and Guo, 2021; Guo et al., 2022; Wallis et al., 2022; Gnesda et al., 2022; Schaefer et al., 2021). However, retention due to air–water interfacial adsorption has not been represented in the standard models outlined in the USEPA guidance for determining SSLs (USEPA, 1996). Not accounting for the additional retention processes at the air–water interfaces can lead to overly conservative (i.e., low) SSLs. Recently, Brusseau and Guo (2023) proposed a revision to the simplest DAF approach in the USEPA SSL framework for determining SSLs for PFAS. The revised approach considers the adsorption of PFAS at the air–water interfaces when converting the porewater concentration to a soil concentration. They showed that accounting for the air–water interfacial adsorption in this mass distribution increases the SSLs by up to an order of magnitude, depending on the type of PFAS. The increase is greater for PFAS with longer carbon chains. However, the revision proposed by Brusseau and Guo (2023) is based on the simplest DAF approach by USEPA that does not account for any attenuation in the vadose zone; the USEPA SSL guidance states that the DAF approach assumes "soil contamination extends to the water table, eliminating attenuation processes in the unsaturated zone" (USEPA, 1996). To our knowledge, the PFAS-specific attenuation processes in the vadose zone have not been represented in any transport models for the purpose of determining SSLs for PFAS-contaminated sites.

We develop a new integrated modeling framework by combining an analytical vadose-zone transport model that includes PFAS-specific retention and transport processes with a relatively simple approach that accounts for the dilution of PFAS by mixing in groundwater. This framework can be used to inversely derive site-specific SSLs for PFAS from a given MCL or another acceptable concentration at a receptor point (i.e., drinking water well) as well as to estimate the PFAS concentration at a receptor well over time in a forward mode to assess the groundwater-contamination risk of a given site. The vadose-zone model is based on recently developed analytical solutions for an advection–dispersion equation that accounts for the adsorption of PFAS at air–water and solid–water interfaces (Guo et al., 2022), which were derived from simplifying the comprehensive mathematical model reported in Guo et al. (2020). Because our vadose-zone model solves a differential equation that represents the retention and transport processes of PFAS, it explicitly accounts for PFAS attenuation in the vadose zone. For groundwater, we employ the simple dilution factor approach reported in the USEPA SSL framework (USEPA, 1996), which assumes that the contaminants discharged to groundwater are well mixed between the leaching location and a receptor well. We demonstrate how this integrated modeling framework can be applied in a range of site-specific applications in both forward and inverse modes.

2. Modeling framework

2.1. Conceptual framework

At contaminated sites, PFAS migrate downward through the vadose zone to impact groundwater, driven by infiltration events (Fig. 1). Given the mass of PFAS in the soil at a contaminated site, it is critical

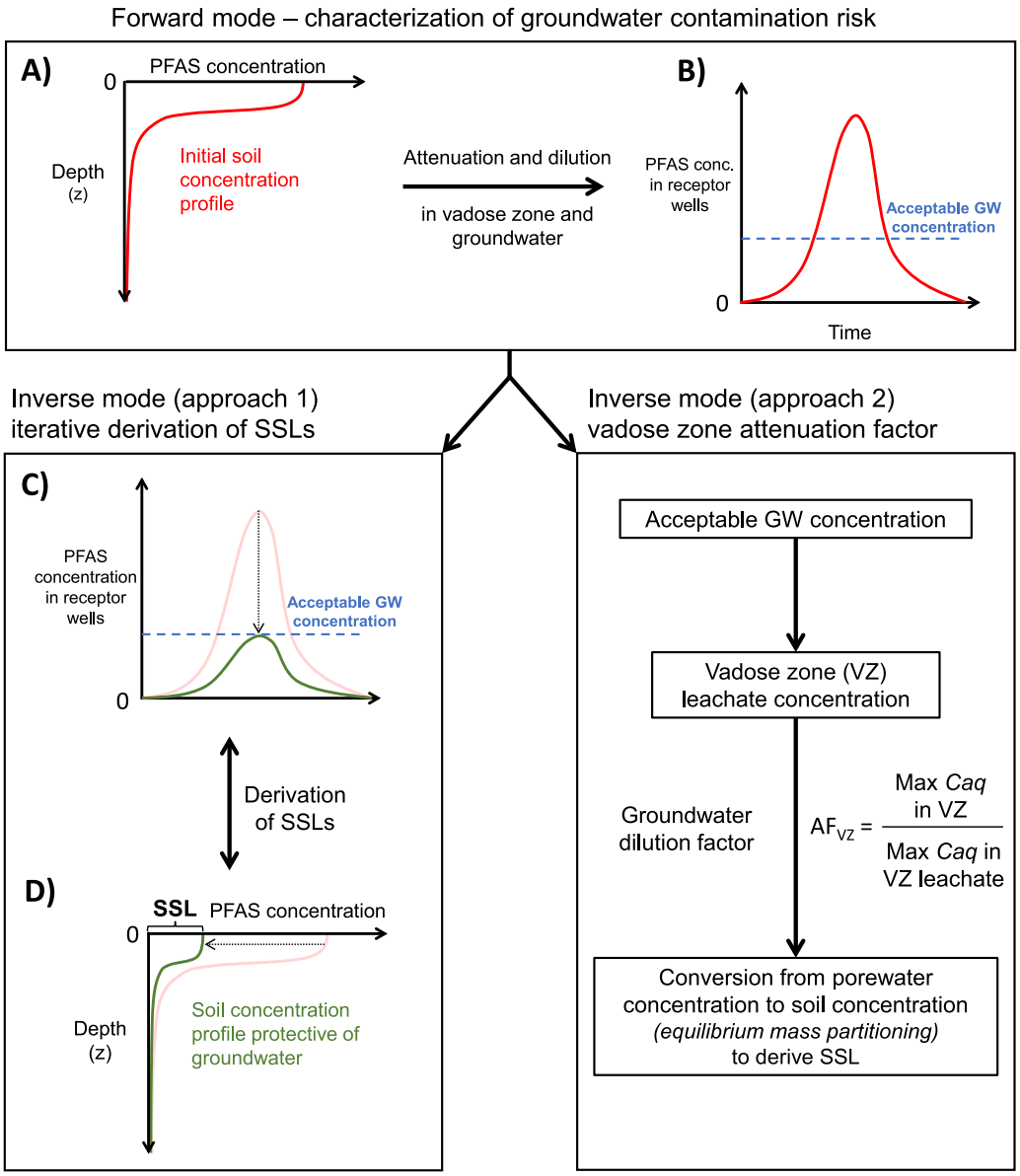

Fig. 2. Schematic for the application of the integrated analytical modeling framework in both forward and inverse modes. The forward mode characterizes contamination risk to groundwater by comparing the predicted concentration in a groundwater receptor well to an MCL or another acceptable concentration. The first approach in the inverse mode iteratively derives a site-specific SSL for a given contaminated site that is protective of the groundwater in a receptor well. The second approach computes a site-specific groundwater dilution factor, and a vadose-zone attenuation factor (derived from the forward mode) to derive the SSL following our recently revised USEPA DAF approach (Brusseau and Guo, 2023).

to predict PFAS concentrations in a receptor well to assess the risks of contamination. Concomitantly, it is also important to derive SSLs for a contaminated site that are protective of the groundwater in a receptor well (i.e., not exceeding the MCLs or other acceptable concentrations). For traditional non-interfacially-active contaminants, the USEPA has published a standard soil screening guidance (USEPA, 1996). As discussed in Section 1, the unique interfacially-active properties distinguish PFAS from traditional non-interfacially-active contaminants and, as a result, the previous USEPA soil screening guidance may not apply to many PFAS. In the present study, we develop an integrated modeling framework comprising a vadose-zone model that incorporates the PFAS-specific transport processes in soils and a groundwater model that uses a simple dilution factor approach to account for PFAS dilution due to mixing in the aquifer.

This integrated framework possesses both forward and inverse modeling modes. Given the soil contamination conditions at a site (Fig. 2A), the forward modeling mode simulates the mass discharge rates at the bottom of the vadose zone which is then input into a groundwater dilution factor model to compute PFAS concentrations at a groundwater receptor well. Comparing the computed PFAS concentration to the MCLs or other acceptable concentrations allows one to determine the risks of groundwater contamination at the site (Fig. 2B). This forward mode can also be used to characterize and quantify the impact of remedial actions designed to reduce mass discharge to groundwater.

Conversely, the inverse modeling mode derives site-specific SSLs that are protective of groundwater at a contaminated site. We present two approaches for the inverse modeling mode. In the first approach, we take the initial soil profile of PFAS concentrations of a contaminated site and incrementally remove PFAS mass in the vadose zone (Fig. 2D) until the PFAS concentration in the groundwater receptor well complies with the MCLs or other acceptable concentrations (Fig. 2C). The remaining upper-bound PFAS concentration in the vadose zone would represent a site-specific SSL. To illustrate this first inverse modeling approach, we present an example wherein the PFAS mass is removed

proportionally across the soil concentration profile (i.e., the shape of the soil concentration profile is kept unchanged) until the PFAS concentration in the groundwater is below the MCL or another acceptable concentration (Fig. 2D).

The second inverse modeling approach is simpler and more direct, which involves two steps. First, we use the forward modeling mode to derive an attenuation factor in the vadose zone. This is done by taking the ratio between the maximum porewater concentration in the vadose zone and the maximum concentration in the soil leachate discharged to groundwater at the bottom of the vadose zone. This ratio would represent the attenuation that PFAS experience leaching through the vadose zone. After obtaining the vadose-zone attenuation factor, we then incorporate the determined attenuation factor into our recently revised USEPA DAF approach (Brusseau and Guo, 2023) to compute an SSL for a given PFAS. The following subsection discusses more details of the vadose-zone and groundwater models. For simplicity, hereafter we will use the MCL as an example acceptable concentration in groundwater, but we note that other types of acceptable groundwater concentrations can also be used in our analytical modeling framework.

2.2. Analytical process-based transport model in the vadose zone and dilution factor model in groundwater

We employ a simplified, analytical model developed by Guo et al. (2022) to model PFAS leaching in the vadose zone. The analytical framework accounts for PFAS-specific transport processes and is designed to be a screening-level tool similar to the simplified tools described in the USEPA soil screening guide (USEPA, 1996). The analytical vadose-zone PFAS leaching model (Guo et al., 2022) adopts the following assumptions: (1) one-dimensional, steady-state water infiltration in a homogeneous vadose zone; (2) linear adsorption at solid–water and air–water interfaces, where a two-domain model is used to represent kinetic solid-phase adsorption and the air–water interfacial adsorption is assumed instantaneous; (3) partitioning to the air phase is not represented; and (4) production of PFAS due to the transformation of precursor is not considered. More details about the analytical solutions and the underlying assumptions are reported in Guo et al. (2022).

We comment on some implications of the assumptions presented above. Prior studies have shown that steady-state flow may be an appropriate assumption for quantifying long-term leaching of PFAS, even in highly heterogeneous vadose zones (Guo et al., 2022; Zeng and Guo, 2023). The assumption of a homogeneous vadose zone suggests that the analytical model may not directly apply to highly heterogeneous vadose zones where PFAS leaching may be strongly influenced by preferential flows (Zeng and Guo, 2023). However, ensembles of multiple model runs of a homogeneous vadose zone covering a wide range of soil properties may be used to indirectly account for the impact of vadose-zone heterogeneity on PFAS leaching and the derived SSLs. We note that while the vadose-zone PFAS leaching model assumes a homogeneous vadose zone, it allows for any spatially varying (or uniform) initial PFAS concentrations in the vadose zone as demonstrated by Guo et al. (2022) as well as in the present study (depth-dependent PFAS concentrations are used as initial concentrations in Section 3.1). Neglecting partitioning to the air phase should be valid for most ionic PFAS that are non-volatile, but may lead to overestimated aqueous-phase leaching for those volatile non-ionic PFAS. Not accounting for precursor transformation may underestimate the leaching of the produced terminal PFAS. One conservative approach to account for that is to assume all of the precursors at the site transform into the terminal PFAS and use greater initial concentrations of the terminal PFAS accordingly based on the initial mass of precursors at the site. Finally, we point out that the analytical PFAS leaching model is not intended to replace more sophisticated mathematical models. As more information and datasets become available at the contaminated sites, more sophisticated models that account for additional transport mechanisms such as nonlinear and non-equilibrium processes and vadose zone heterogeneities (e.g., Guo et al., 2020; Zeng et al., 2021; Zeng and Guo, 2021, 2023) may be used for more advanced and detailed analysis.

The analytical vadose-zone PFAS leaching model provides spatial PFAS concentration profiles over time as well as time-dependent mass discharge rates at the bottom of the vadose zone. Additionally, it can also be used to derive an effective vadose-zone attenuation factor representing the detailed attenuation processes occurring in the vadose zone. We define the vadose-zone attenuation factor as the ratio between the maximum porewater concentration in the vadose zone and the maximum leachate concentration discharged to groundwater at the bottom of the vadose zone. It is noted that this attenuation factor does not incorporate dilution within groundwater, which is represented separately in the groundwater dilution factor model discussed below. The vadose-zone attenuation factor is expected to be a function of various factors, including soil properties, PFAS interfacial activity, and infiltration conditions.

PFAS discharge rates computed by the vadose-zone model are passed onto the groundwater model to determine the PFAS concentration in a receptor point (e.g., drinking water well) downstream of the source zone. In the present study, we employ a simple dilution factor model that assumes well-mixed conditions in the aquifer between the PFAS mass discharge location and the receptor well, following that used in the USEPA soil screening guidance (USEPA, 1996) and a few other studies (Connor et al., 1997; Anderson, 2021). This simple dilution factor approach only accounts for contaminant dilution in groundwater and hence neglects any potential attenuation that may occur during transport in groundwater. The dilution factor (USEPA, 1996) can be computed as

$$DF = 1 + \frac{U_{gw}\delta_{gw}}{I_f W}, \tag{1}$$

where U_{gw} is the groundwater Darcy velocity (cm/yr). I_f represents annual net infiltration (cm/yr). W is the lateral width of the contaminated site (cm). δ_{gw} represents a computed estimate for the thickness of the groundwater mixing zone (cm), which is calculated using the following equation

$$\delta_{gw} = \sqrt{2\alpha_v W} + b_{sat}\left[1 - \exp\left(\frac{-I_f W}{U_{gw} b_{sat}}\right)\right], \tag{2}$$

where the vertical groundwater dispersivity α_v is estimated as 0.0056*W, and b_{sat} represents the saturated thickness of the water-bearing unit (cm). By definition, δ_{gw} cannot exceed b_{sat}.

Note that when limited information about the contaminated site is available for computing a site-specific DAF, e.g., when using the SSL framework for national applications, the USEPA soil screening guidance recommends a default DAF of 20 to account for contaminant dilution and attenuation during transport from the source zone to a groundwater receptor point. It is interesting to note that the current USEPA Reference Tables for regional SSLs even assume a DAF of 1 for certain conditions (USEPA, 2023b) (accessed in January 2024).

The integrated modeling framework requires an array of site-specific parameters as inputs into the mathematical models. These include soil hydraulic and geochemical parameters, PFAS properties, and other site-specific information such as depth to the groundwater table, the spatial distribution of initial PFAS concentration, and infiltration conditions. The soil parameters include residual water content θ_r, saturated water content θ_s, parameters for the soil water characteristics (e.g., van Genuchten parameters α and n), soil bulk density ρ_b, and saturated hydraulic conductivity K_s. Parameters for the PFAS properties include interfacial activity parameters (e.g., Szyszkowski parameters a and b), solid-phase adsorption coefficients, and aqueous molecular diffusion coefficients. Site-specific parameters include infiltration, depth to groundwater table, size of the source zone, and PFAS concentrations. The other critical parameter for PFAS transport is the air–water interfacial area. Several approaches can be employed to

Table 1
Parameter values for the 9 PFAS selected for the two constructed contaminated sites. Six PFAS are perfluoroalkyl carboxylic acids (PFCAs), and the other three PFAS are perfluorosulfonic acids (PFSAs). The biosolids loading rates are derived from Venkatesan and Halden (2013). a and b are the Szyszkowski parameters obtained from the surface tension data reported by Silva et al. (2019) and Silva et al. (2021), as summarized in Guo et al. (2022). M is the molecular weight of PFAS. The diffusion coefficients D_0 are obtained from Schaefer et al. (2019b). The MCLs for PFOA and PFOS are obtained from the EPA proposed MCLs (USEPA, 2023a), and those for PFNA, PFBS, and PFHxS are simplified for individual PFAS from the Hazard Index MCL (USEPA, 2023a). The MCLs for the other PFAS are then estimated based on their carbon-chain length relative to that of the PFAS included in the USEPA's proposal MCLs. Note that the assumed MCLs are used as an example to illustrate the application of the analytical modeling framework; other types of acceptable groundwater concentrations can also be used.

PFAS	a mg/L	b –	M g/mol	D_0 ($\times 10^{-6}$) cm^2/s	Biosolids Release rate μg/cm^2/yr	AFFF Release Rate μg/cm^2/yr	Assumed MCL μg/L
PFPeA	3168.6	0.22	264.05	12	0.000548	0.385	2
PFHxA	1350.42	0.21	314.05	7.8	0.00103	1.257	2
PFHpA	345.86	0.22	364.06	9.3	0.000567	0.503	2
PFOA	62.11	0.19	414.07	4.9	0.00567	1.509	0.004
PFNA	5.11	0.16	464.08	2.93	0.00153	0.00519	0.01
PFDA	3.7	0.17	514.08	2.27	0.00435	0.00251	0.004
PFBS	2400.8	0.15	300.1	11	0.000567	2.347	2
PFHxS	160.05	0.14	400.12	4.5	0.000984	11.902	0.009
PFOS	3.65	0.12	500.13	5.4	0.0672	167.628	0.004

quantify or estimate the air–water interfacial area as a function of water saturation for a soil medium spanning from advanced direct X-ray micro-tomography imaging to indirect interfacially-active tracer methods to simpler approaches that estimate the air–water interfacial area using the soil hydraulic properties or information of soil grain size as recently reviewed by Brusseau (2023). In the present study, we employ the commonly used thermodynamic-based method to estimate the air–water interfacial area as a function of water saturation, as was done in Zeng et al. (2021) and Guo et al. (2022). In this approach, the air–water interfacial area can be estimated using only parameters related to the soil water characteristics (Leverett, 1941; Morrow, 1970; Bradford and Leij, 1997).

$$A_{aw} = \frac{\phi}{\sigma} \int_{S_w}^{1} p_c\left(S_w\right) \mathrm{d}S_w, \tag{3}$$

where ϕ is the porosity of the soil, σ is the surface tension of water, p_c is the capillary pressure, and S_w is water saturation. When computing the thermodynamic-based A_{aw}, the surface tension σ in Eq. (3) is taken as the surface tension with no dissolved PFAS. Prior studies suggest that the thermodynamic-based method may underestimate the air–water interfacial area compared to that measured by aqueous interfacial tracers (Jiang et al., 2020; Brusseau, 2023), likely due to not representing the impact of soil grain surface roughness. A scaling factor has been proposed to correct the thermodynamic-based A_{aw} (Zeng et al., 2021; Guo et al., 2022; Silva et al., 2022; Brusseau and Guo, 2023; Brusseau, 2023). Brusseau (2023) developed multiple approaches for estimating the roughness scaling factor depending on different levels of data availability. We point out that, in addition to the thermodynamic-based A_{aw} that needs the soil water characteristics as input, there are also other even simpler approaches available that only require readily available basic information, such as specific solid surface area and median grain diameter of the porous medium (Brusseau, 2023).

3. Example applications

3.1. Application to assessing contamination risks and deriving SSLs

We present example applications to demonstrate how our integrated modeling framework can be applied to assess contamination risks and derive SSLs from a given acceptable groundwater concentration. We construct two common types of PFAS-contaminated sites (Fig. 3). The first is representative of a fire-fighting training area site impacted by PFAS-containing aqueous film-forming foams (AFFFs). The second represents an agricultural site impacted by the application of PFAS-contaminated biosolids (Pepper et al., 2021; Sepulvado et al., 2011; Moodie et al., 2021). The two sites have some key differences, including PFAS concentration levels, the amount of water infiltration due to different operational conditions, and the size of the site footprint. To focus on examining the impact of these differences, we consider the same suite of soils and PFAS, depths of the vadose zone, and the same range of precipitation for these two sites. More details about the two sites are presented below.

We synthetically generate PFAS contamination at the two sites by simulating their respective contamination scenarios, i.e., the release of PFAS to the vadose zone by fire training and biosolids application. The fire training and biosolids application are both assumed to last 30 years. For both sites, we consider nine representative PFAS with varying carbon-chain lengths and head groups (Guo et al., 2022). The parameters for the list of PFAS are summarized in Table 1. See additional information for the determination of these parameters in Guo et al. (2022). The release rates of PFAS at the two sites are determined as follows. The AFFF-impacted site uses fire training operations and PFAS concentrations in the AFFF solution similar to those reported in the literature that follow standard practices at fire training area sites (Guo et al., 2020; Zeng et al., 2021; Guo et al., 2022). The fire training is assumed to occur every ten days, each session lasting 30 min (total infiltration of 0.0458 cm of 1% diluted AFFF solution during each session). The PFAS concentrations in the 1% AFFF solution are obtained from Høisæter et al. (2019). For the biosolid site, we assume an average annual loading rate of 6.75 dry tons per acre, derived from a USEPA technical report (USEPA, 2000). From Venkatesan and Halden (2013), we derive the respective PFAS concentrations present in the biosolids, and then use the average dry weight and PFAS concentrations to obtain the estimated annual loading rate of PFAS for the synthetic biosolids sites.

For both sites, we consider 6 different soils spanning from sand to sandy clay loam (Nguyen et al., 2020; Guo et al., 2022). The soil hydraulic parameters are listed in Table 2 and the solid-phase adsorption parameter for each PFAS specific to the different soils are in Table 3. The K_d values represent the mean K_d across the entire depth of the vadose zone. We assume that the measured K_d values reported in Nguyen et al. (2020) represent the soils in the top 0.6 m of the vadose zone. Assuming the remaining depth of the vadose zone has significantly less organic carbon (i.e., 20% of that in the shallow soil) based on field observations (Schaefer et al., 2021), we obtain the mean K_d through arithmetic averaging. When estimating the mean K_d, we assume that adsorption to organic carbon is the main contributor to solid-phase adsorption. For the estimation of the air–water interfacial area, we set the surface roughness scaling factor to 1 for simplicity. As discussed earlier in Section 2, using a surface roughness scaling factor of 1 would represent an underestimated air–water interfacial area and subsequently smaller retention in the soil, which can be viewed as a conservative approach for assessing groundwater contamination risks.

Three levels of annual precipitation (30 cm, 60 cm, and 120 cm) are considered, covering semi-arid to much wetter climates. The precipitation needs to be converted to effective net annual infiltration.

Table 2
Hydraulic and transport parameters for the six soils employed in the example applications. Most of the parameters were reported in Guo et al. (2022). The soil texture information is obtained from Nguyen et al. (2020). Using the United States Department of Agriculture classification, the six selected soils are classified as sand, sandy loam, two loams, sandy clay, and sandy clay loam, respectively. The hydraulic parameters including saturated conductivity K_s, saturated water content θ_s, residual water content θ_r, and the Van Genuchten parameters α and n are estimated by the Rosetta pedotransfer model (Zhang and Schaap, 2017). The dispersion coefficient α_L is approximated using the empirical model of Xu and Eckstein (1995) and is assumed independent of water saturation. Note that the predicted K_s values reported in Guo et al. (2022) were inadvertently mixed for the last four soils. Those values have been corrected here.

Soil	K_s cm/day	θ_s cm^3/cm^3	θ_r cm^3/cm^3	ρ_b g/cm^3	α cm^{-1}	n –	α_L cm
Sand	482.7	0.363	0.054	1.58	0.03133	2.72	24.39
Sandy Loam	211.1	0.570	0.097	0.82	0.01291	1.38	24.39
Loam 1	10.1	0.361	0.079	1.59	0.01072	1.362	24.39
Loam 2	16.2	0.384	0.079	1.47	0.00893	1.411	24.39
Sandy Clay	6.1	0.383	0.111	1.66	0.01364	1.238	24.39
Sandy Clay Loam	8.2	0.371	0.090	1.59	0.01095	1.327	24.39

Table 3
Solid-phase adsorption coefficients K_d for the nine PFAS in the six soils used in the present study. The K_d values represent the mean K_d across the entire depth of the vadose zone. The K_d in the shallow soil (top 0.6 m) are obtained from Nguyen et al. (2020), and the values in the deeper vadose zone are estimated assuming lower organic carbon fractions (20% of that in the shallow soil). The K_d values for Sandy Loam are generally much greater than that of the other soils due to its much greater organic carbon content (Nguyen et al., 2020).

PFAS	K_d (cm^3/g)					
	Sand	Sandy Loam	Loam 1	Loam 2	Sandy Clay	Sandy Clay Loam
PFPeA	0.013	0.141	0.064	0.048	0.077	0.112
PFHxA	0.016	0.166	0.067	0.054	0.077	0.112
PFHpA	0.096	0.451	0.150	0.147	0.160	0.195
PFOA	0.170	0.909	0.454	0.205	0.259	0.218
PFNA	0.406	3.421	0.566	0.640	0.419	0.502
PFDA	2.410	14.64	2.547	3.936	5.398	0.275
PFBS	0.016	0.160	0.064	0.054	0.080	0.115
PFHxS	0.090	0.678	0.125	0.144	0.128	0.221
PFOS	1.030	10.976	1.126	1.338	1.008	1.104

Here, we employ a simple scaling equation suggested by Stephens et al. (1996) and Connor et al. (1997) that estimates net infiltration from precipitation for sandy soils without having to gather detailed information on site properties like impervious surface cover, curve number, or vegetation at a specific site if this information is not available. In this approach, the effective net annual infiltration rate $I_f = 0.0018p^2$ (cm/yr), where p is net annual precipitation (cm/yr). With this estimation method, 30 cm, 60 cm, and 120 cm of net annual precipitation lead to 1.62 cm, 6.48 cm, and 25.92 cm of effective net annual infiltration, respectively. A variety of approaches spanning different levels of complexity and data availability for estimating net recharge are reported in the literature (e.g., Scanlon et al., 2002; Healy, 2010), including a recent review by Newell et al. (2023) in the context of quantifying PFAS mass discharge from unsaturated source zones. Those approaches can also be incorporated into our integrated modeling framework (see Fig. 3).

The two types of contaminated sites have a few important differences. Fire training areas vary in size, but are often relatively small in area, spanning between approximately 100 m^2 and 2000 m^2 (FAA, 2010). At these sites, decades of fire training using AFFF products results in highly-contaminated vadose zones (Anderson et al., 2019; Brusseau et al., 2020). As an example, we consider a synthetic AFFF-impacted fire training site of 30 by 30 m (FAA, 2010) and simulate the release of PFAS-containing AFFF to the vadose zone due to regular fire training over 30 years. The depth of the vadose zone is assumed 400 cm. The AFFF release rates and the concentrations of PFAS in the 1% diluted AFFF solution were determined based on previous studies (Guo et al., 2020; Høisæter et al., 2019; Zeng et al., 2021). Because we assume steady-state water infiltration in the vadose zone, the release rates of PFAS are averaged annually (see Table 1). For the estimation of the groundwater dilution factor, we assume a site dimensionality (W) of 30 m, groundwater Darcy velocity U_{gw} of 1 m/day, and aquifer saturated thickness (b) of 3.05 m. Note that these numbers are estimated values for our synthetic scenarios used to demonstrate the modeling framework. They need to be site-specific when the modeling framework is applied to real-world sites.

Agricultural sites impacted by the application of PFAS-containing biosolids are typically much larger than AFFF-impacted fire training area sites, often spanning over 1,000 acres. Biosolids are usually applied once or twice per year and the PFAS concentrations in the biosolids are typically several orders of magnitude lower than that in the diluted AFFF solutions. We assume 6.5 dry tons per acre, or 0.1513 g/cm/yr, of biosolids are applied annually based on the USEPA-recommended loading rates averaged for all crop types (USEPA, 2000). The concentrations of PFAS in the biosolids in terms of mass per dry weight are obtained from Venkatesan and Halden (2013). The PFAS concentrations in the biosolids are multiplied by the biosolids loading rates to obtain the PFAS release rate in Table 1. Note that here we have not accounted for any additional retention of PFAS by the biosolids materials, which may be considered as a "worst-case" scenario for assessing groundwater contamination risks. The depth of the vadose zone is assumed the same as the fire training area site for comparison. Due to the much larger area, we assume a site dimensionality (W) of 2,354 m corresponding to an area of approximately 1,369 acres, i.e., the average farm size in Arizona (USDA, 2020).

The other major difference between the AFFF and biosolids sites is the net annual infiltration. In addition to precipitation, agricultural sites may have additional infiltration due to irrigation. Based on information reported by the United States Department of Agriculture (USDA-NASS, 2019), we assume an average annual irrigation rate of 45.72 cm of water per year, equivalent to the reported average irrigation rate of 1.5 ft. Assuming 20% of the irrigated water reaches the groundwater, we obtain 9.144 cm of additional net infiltration due to irrigation. This irrigation-induced infiltration is added to the net infiltration due to precipitation to obtain the total net infiltration for the biosolids sites.

To keep the generated PFAS concentration profiles the same for each PFAS and soil type when used for different precipitation rates, we use constant precipitation of 30 cm when generating the synthetic concentration profiles for the two contaminated sites. Having the same starting soil PFAS concentration profile makes it easier to

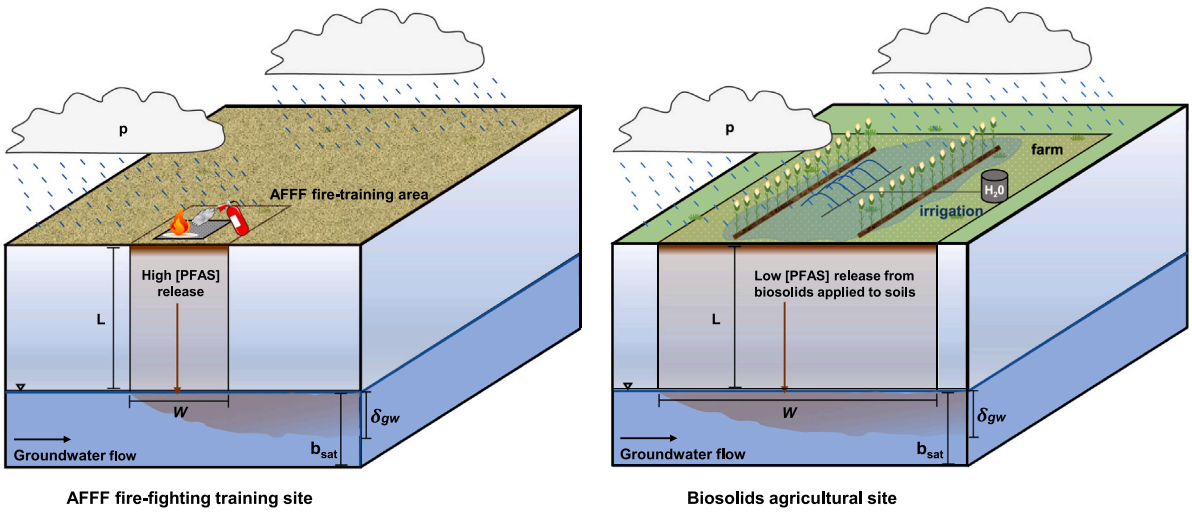

Fig. 3. Conceptual models detailing the two types of example contaminated sites being analyzed in the present study. The key differences between the AFFF-impacted fire training site and the agricultural site receiving PFAS-containing biosolids are: site footprint, soil PFAS concentrations (i.e., the amount of PFAS released to the subsurface), and infiltration rates.

examine the impact of the different infiltration rates on groundwater contamination risks and SSLs. Combining 9 individual PFAS and 6 soil types generates 54 synthetic contamination cases for each of the two types of contaminated sites. These synthetic soil PFAS contamination profiles are used to demonstrate the application of our SSL framework at PFAS-contaminated sites under a wide range of conditions.

3.2. Additional considerations for the application of the modeling framework

In addition to the specific data availability in the example applications discussed above, the analytical modeling framework can also be applied to situations with a different level of data availability. For instance, while synthetic high-resolution initial PFAS concentration profiles are used in the above examples, the analytical modeling framework can also be applied to general soil concentration profiles with any number of depth-discrete data points collected from a contaminated site. The minimal number of depth-discrete samples required to represent a vadose zone will depend on the vertical variability of PFAS concentrations. For example, a vadose zone with highly depth-dependent PFAS concentration will likely need more depth-discrete samples than that for a vadose zone with a relatively uniform PFAS concentration. In practical applications, users may need to make decisions based on the specific site conditions and use the modeling framework (by running different scenarios) to test whether adding more depth-discrete samples would appreciably change the computed results (e.g., PFAS concentrations at the receptor point or the derived SSL*s*).

Additionally, soil water characteristic parameters are used to determine the soil water content and the air–water interfacial area in the example applications, but these two parameters can also be obtained from other approaches if the soil water characteristic parameters are not available. For example, the soil water content can be measured from the soil samples of soil borings. The air–water interfacial area can also be estimated from other more readily available information, such as the specific solid surface area and medium grain diameter, as discussed in Brusseau (2023). Furthermore, PFAS porewater concentration datasets collected by suction lysimeters have recently become more commonly available at PFAS-contaminated sites (Quinnan et al., 2021; Schaefer et al., 2022; Anderson et al., 2022; Schaefer et al., 2023). These porewater concentration datasets can potentially be used to further constrain the model parameters related to PFAS retention in the vadose zone as suggested by Anderson (2021).

The examples applications in Section 3.1 focus on the assessment of contamination risks and the determination of SSLs, which are critical for the initial stages of site investigations to prioritize sites for further characterization. However, the analytical modeling framework can also be used for more general applications. For example, it can be used to characterize the source strength and long-term impacts of PFAS leaching and mass discharge to groundwater. It can also be used to evaluate the effectiveness of different remediation strategies such as partial source removal or installation of a horizontal barrier, e.g., source removal can be represented by modifying the initial PFAS concentration profile. It is important to note that because the analytical modeling framework is computationally efficient, any uncertainties in the input parameters or datasets can be propagated to the model predictions using Monte Carlo-type simulations. Overall, it is anticipated that the analytical modeling framework will be useful for a variety of site characterization and remedial selection/assessment efforts, and lead to an improved capacity to determine, manage, and mitigate risks associated with PFAS-contaminated sites.

4. Results and discussion

We present simulation results and analyses to demonstrate how the analytical modeling framework can be used to characterize groundwater contamination risks for a given contaminated site and to determine site-specific SSLs that are protective of an adjacent groundwater receptor well, using the two example types of contaminated sites discussed in Section 3.1.

4.1. Characterize PFAS contamination risks in groundwater

As discussed in Sections 1 and 2, PFAS in the vadose zone experience additional retention due to adsorption at fluid–fluid interfaces (e.g., air–water interfaces) compared to traditional non-interfacially-active contaminants. To illustrate the impact of these additional retention processes, we use the analytical vadose-zone transport model to simulate the transport and quantify the attenuation of PFAS in the vadose zone and their concentrations in a groundwater receptor well impacted by the source zone. The effective attenuation factor, as defined in Section 2, represents the ratio of the maximum PFAS porewater concentration in the vadose zone to the maximum concentration discharged to groundwater, which can be computed by operating the analytical vadose-zone transport model in a forward mode. A greater attenuation factor indicates greater retention experienced by that PFAS in the vadose zone.

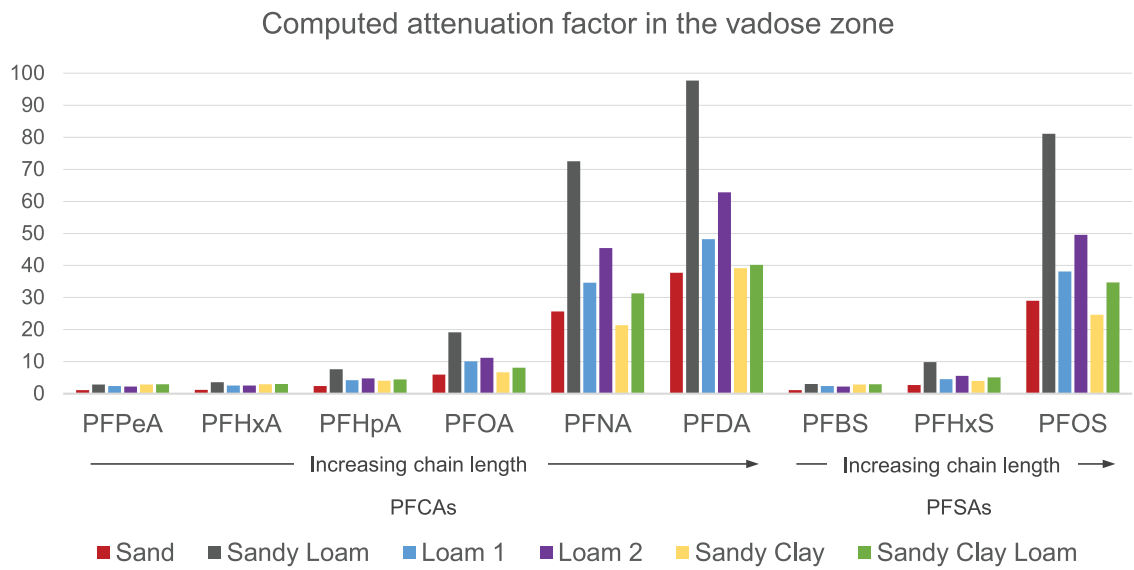

Fig. 4. Computed attenuation factors for the 9 PFAS in the vadose zone for the AFFF-impacted fire training site at a precipitation level of 60 cm. The greater attenuation factors for the sandy loam are due to their much greater solid-phase adsorption capacity compared to the other soils (see Table 3). (For interpretation of the references to color in this figure legend, the reader is referred to the web version of this article.)

The computed effective attenuation factors for the nine PFAS in the vadose zone are presented in Fig. 4. The AFFF-impacted fire training site at a precipitation level of 60 cm is used as an example. The results indicate a strong dependence of the vadose-zone attenuation factor on the specific PFAS. For the same soil, the vadose-zone attenuation factor can vary by up to almost two orders of magnitude among PFAS, and it increases for PFAS with a longer carbon chain for both PFCAs and PFSAs. The attenuation factors for the shorter chain PFAS are close to 1, indicating minimum retention experienced in the vadose zone. Because the shorter-chain PFAS experience minimum retention, their attenuation factors are much less sensitive to the soil media. Conversely, the attenuation factor for the longer-chain PFAS varies strongly among the different soil media. For example, the attenuation factors for PFNA, PFDA, and PFOS are consistently greater than 20 for all six soils. It is interesting to note that the attenuation factors for the Sandy Loam soil are much greater than the other soils. A closer inspection reveals that the larger attenuation factors are caused by the Sandy Loam soil's greater solid-phase adsorption capacity compared to the other soils (see Table 3).

The attenuation factors for the PFAS in the vadose zone directly influence the mass discharge rates to groundwater and the PFAS concentration at receptor points in groundwater (e.g., groundwater receptor wells). Fig. 5 shows the simulated PFAS concentrations in a groundwater receptor well impacted by the source zone, which represents potential groundwater contamination risks. The case of the Sandy Clay Loam soil for the AFFF-impacted fire training site under all three precipitation levels is presented as an example. The significant differences in the PFAS concentrations under different precipitation levels demonstrate that precipitation and net infiltration are major drivers of PFAS leaching from the vadose zone to groundwater. As expected, at lower precipitation levels (i.e., smaller net infiltration), the receptor well has lower peak concentrations, and the duration of the leaching process is longer. We also present the results where the vadose-zone transport model does not account for the air–water interfacial adsorption (second row of Fig. 5). Comparisons with the results that account for air–water interfacial adsorption indicate the importance of adsorption of PFAS at the air–water interface as a primary retention mechanism, especially for the longer-chain PFAS. Not accounting for adsorption at the air–water interface accelerates the leaching process and leads to much greater predicted PFAS concentrations in groundwater for the longer-chain PFAS. For example, when air–water interfacial adsorption is not included, the peak concentration for PFOS increases by approximately 7, 4, and 2.5 times for the precipitation levels of 30 cm, 60 cm, and 120 cm, respectively.

The simulated PFAS concentrations in the groundwater receptor well differ significantly between the AFFF-impacted fire training and biosolids-impacted agricultural sites (Fig. 5 vs. Fig. 6). The peak concentrations for the AFFF-impacted site are up to an order of magnitude greater than that for the biosolids site under the same soil conditions, especially for longer-chain PFAS. For example, PFOS peak concentrations for the highest precipitation case differ by a factor of approximately 37. The shorter-chain PFAS also differ on average by a factor of 10 between the two site types. This is because the soils at the AFFF-impacted site generally have much greater PFAS concentrations than those at the biosolids-impacted agricultural site. See Figures S1-10 in the supporting information (SI) for the spatial concentration profiles at the beginning of the leaching simulation for some example cases. For both sites, it is interesting that while the simulated concentrations of PFOS and PFOA in the groundwater receptor well are much greater than their MCLs, some of the shorter-chain PFAS do not exceed their assumed MCLs (Table 1). This is especially true for the biosolids-impacted site where the simulated PFAS concentrations in the groundwater receptor well are generally much lower. Note that this is expected due to the lower soil PFAS concentrations for the biosolids-impacted site relative to that for the AFFF-impacted site.

The simulated PFAS concentrations for the biosolids-impacted site are less sensitive to precipitation levels, but they are still sensitive to the net infiltration rates—the biosolids site receives additional infiltration due to irrigation. PFAS leaching being highly sensitive to the net infiltration rates highlights the importance of quantifying the net infiltration or groundwater recharge for accurately characterizing the contamination risks of PFAS to groundwater resources at PFAS-contaminated sites. The dilution factor in groundwater also has an impact on the PFAS concentrations in the groundwater receptor well. The dilution factor (Eq. (1)) is a function of groundwater velocity, net infiltration rate, contaminated site dimension, and other parameters. The computed dilution factors differ greatly between the two sites due to their different site dimensionalities ($W = 30$ m for the AFFF-impacted fire training site while $W = 2,354$ m for the biosolids-impacted agricultural site). The dilution factors for the biosolids-impacted agricultural site (ranging from 2.3 to 5.9) are much smaller than those for the AFFF-impacted site (ranging from 144 to 2200). It is important to

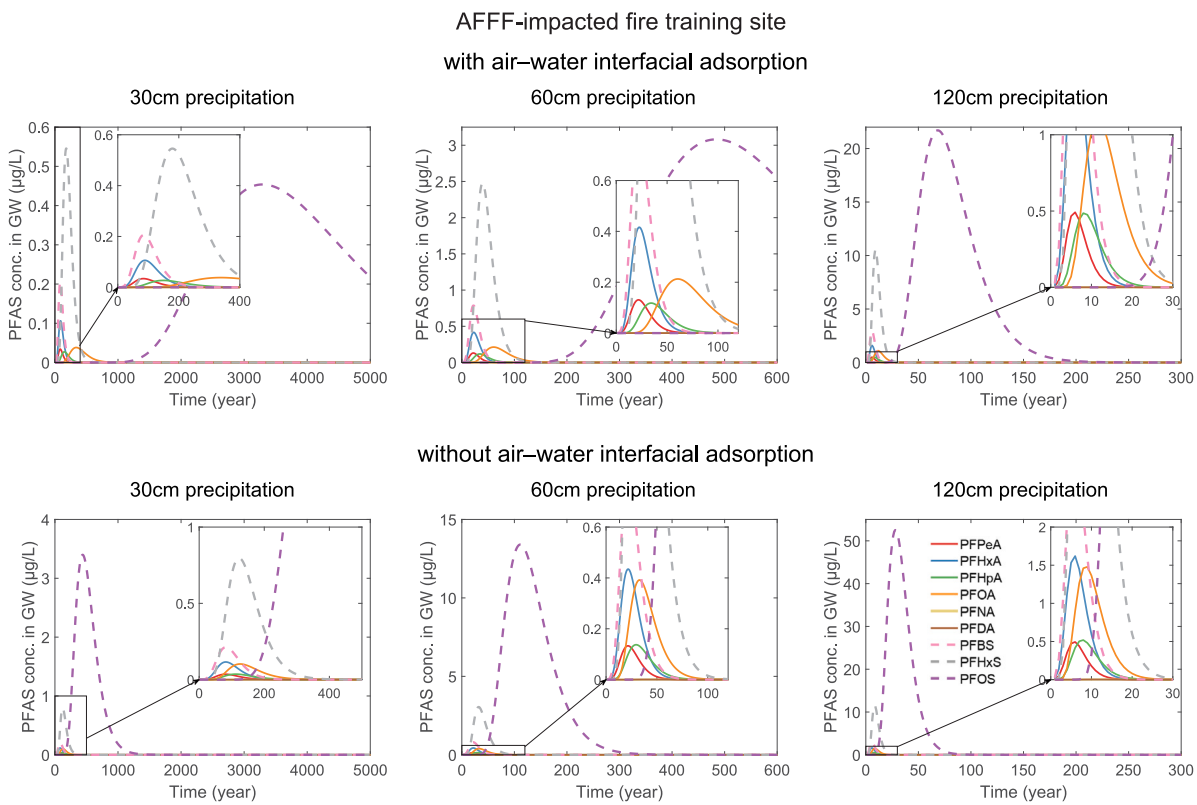

Fig. 5. Simulated concentrations of PFAS in a groundwater receptor well impacted by the source zone of the AFFF-impacted fire training site, with and without accounting for PFAS adsorption at the air–water interfaces. The case of the Sandy Clay Loam soil under all three precipitation levels (30 cm, 60 cm, and 120 cm) is presented. (For interpretation of the references to color in this figure legend, the reader is referred to the web version of this article.)

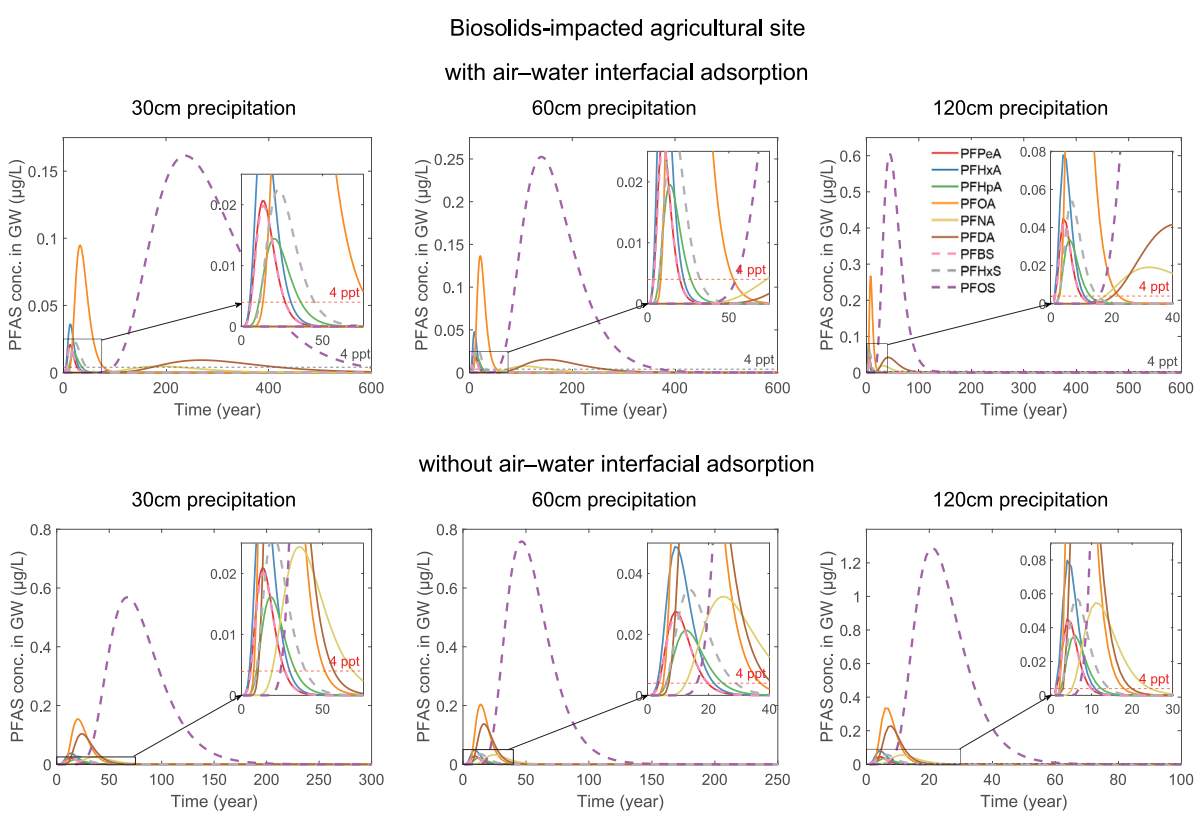

Fig. 6. Simulated concentrations of PFAS in a groundwater receptor well impacted by the source zone of the biosolids-impacted agricultural site, with and without accounting for PFAS adsorption at the air–water interfaces. The case of the Sandy Clay Loam soil under all three precipitation levels (30 cm, 60 cm, and 120 cm) is presented as an example. 4 ppt, the USEPA proposed MCL for PFOS and PFOA (USEPA, 2023a), is shown as a reference. (For interpretation of the references to color in this figure legend, the reader is referred to the web version of this article.)

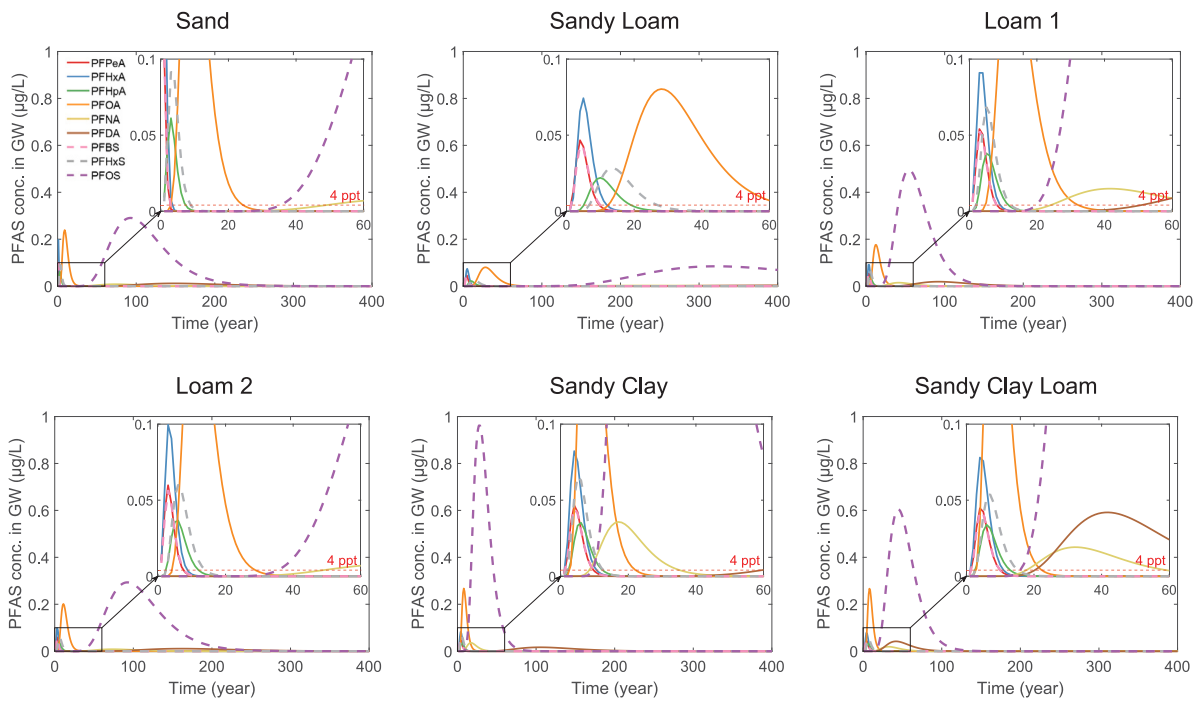

Fig. 7. Simulated concentrations of PFAS in a groundwater receptor well impacted by the source zone of the biosolids-impacted agricultural site for the six different soils. The case of a precipitation level of 120 cm is used as an example. 4 ppt, the USEPA proposed MCL for PFOS and PFOA (USEPA, 2023a), is shown as a reference. (For interpretation of the references to color in this figure legend, the reader is referred to the web version of this article.)

point out that our analytical framework employs the simple dilution factor approach (Eq. (1)) recommended by the USEPA soil screening guidance (USEPA, 1996), but other more sophisticated groundwater flow and transport models that may be more suitable when more site-specific information is available can also be incorporated in our analytical framework in lieu of the currently employed dilution factor model.

For both types of contaminated sites, the properties of the soils in the vadose zone act as primary factors affecting PFAS leaching and the PFAS concentrations in the groundwater receptor well. Fig. 7 compares the computed PFAS concentrations in the groundwater receptor well for all six soil types using the biosolids-impacted agricultural site as an example. The PFAS concentrations in the groundwater receptor well vary among soil types. A closer inspection reveals that the variation is caused by the different solid-phase adsorption capacities and different magnitudes of air–water interfacial area (partly due to the different soil water characteristics of the different soils (Table 2). The Sandy Loam soil appears to have the strongest vadose-zone attenuation for the longer-chain PFAS among all six soils. For example, PFOS begins to enter the groundwater receptor well at approximately 200 years for the Sandy Loam soil, while the PFOS plume has already passed through the groundwater receptor well in a similar timeframe for all the other five soils. Correspondingly, the peak concentration is also between 3 to 9 times smaller than for the other five soils. As mentioned earlier in the discussion of the vadose-zone attenuation factors (Fig. 4), the stronger attenuation is caused by the Sandy Loam soil's much greater solid-phase adsorption capacity relative to the other soils (Table 3). Interestingly, relatively small differences are observed among the other five soils for the concentrations of the longer-chain PFAS in the groundwater receptor well, consistent with the similar leaching behaviors reported in Guo et al. (2022). Finally, we note that the K_d for the six soils in the present study are determined based on measured K_d values. However, measured K_d may not be available for general applications at contaminated sites and may need to be estimated. Rovero et al. (2021) reviewed K_d values for many soils and PFAS and reported that K_d may vary strongly from site to site even for the same soil types. This implies that soil types alone may not be sufficient for estimating K_d, and additional measurements such as geochemical properties will be needed to reduce uncertainties for estimating K_d.

4.2. Inverse framework and derivation of site-specific SSLs for PFAS

In this section, we illustrate how the analytical modeling framework can be used in an inverse mode to determine site-specific SSLs for PFAS. We generate synthetic PFAS-contaminated sites for both the AFFF-impacted fire training and biosolids-impacted agricultural sites that have gone through 30 years of active contamination under a wide range of conditions as described in Section 3.1. PFAS concentration profiles in the vadose zone are taken at the end of this 30-year contamination period. The various corresponding site conditions are then used as example contaminated sites for evaluating the site-specific SSLs for PFAS. Specifically, we take the PFAS concentration profiles and the site conditions and then apply the integrated modeling framework to simulate the PFAS concentration in a groundwater receptor well impacted by the contaminated site. We then compare the simulated peak concentration for each PFAS under consideration to a given MCL. If the simulated peak concentration is lower than the MCL, then the site may be considered not of concern for this specific PFAS with respect to the soil-to-groundwater exposure pathway. Otherwise, further investigation and remedial actions may be required to remove PFAS in the soil to comply with the MCL. For illustrative purposes, we employ a simple approach where we represent a remedial action as the removal of the soil PFAS mass proportionally across the entire soil concentration profile. We then use an iterative approach to derive the site-specific SSL for each PFAS at each specific synthetic contaminated site. Specifically, we incrementally remove a fraction of the soil PFAS mass, re-simulate the PFAS concentration at the receptor well, and then compare the peak concentration with the given MCL. We keep removing the PFAS mass until the peak concentration of PFAS falls below the MCL. The upper-bound soil concentration of the remaining PFAS in the soil may be considered as the soil screening level that is protective of the groundwater at this site. For scenarios where the MCL

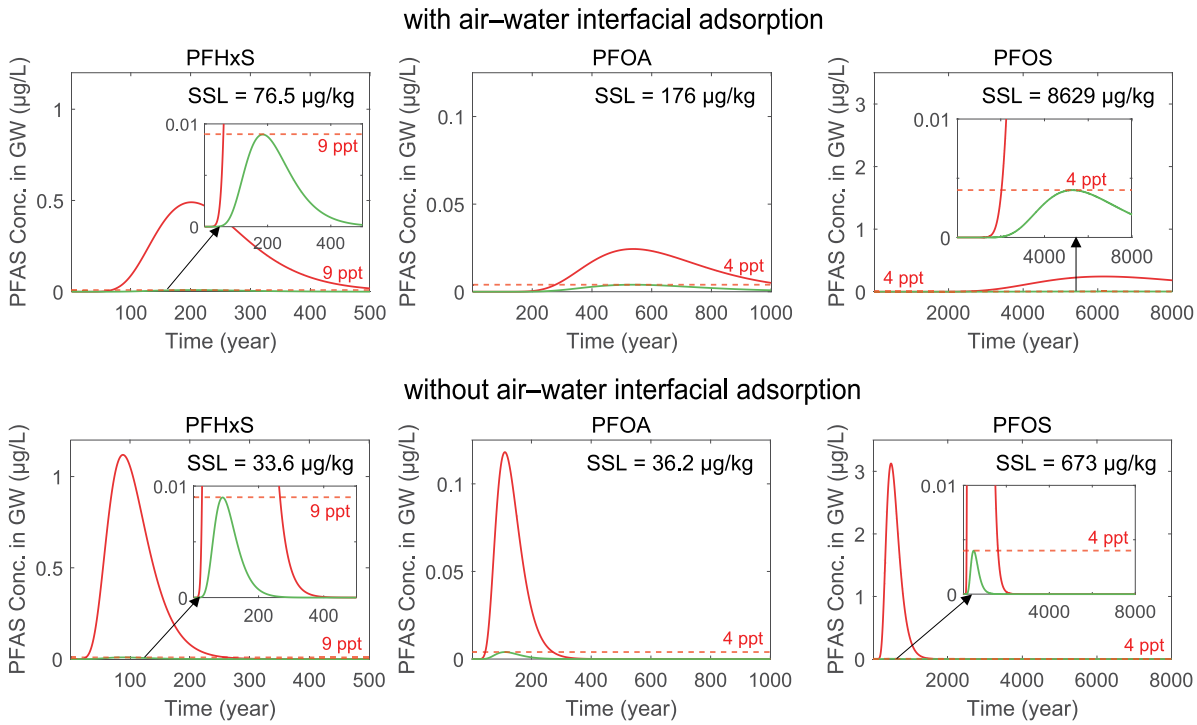

Fig. 8. Illustrative example for the derivation of SSLs using the inverse mode of the integrated modeling framework. The AFFF-impacted fire training site for the case of Loam 2 soil at 30 cm precipitation level is presented for three PFAS (PFHxS, PFOA, and PFOS). The soil concentration of PFAS is iteratively reduced such that the peak concentration in the groundwater receptor well impacted by the contaminated site goes below the MCL (from the red curve to the green curve). Insets are included to zoom in on the comparison with the MCL. The derived soil screening levels with and without accounting for air–water interfacial adsorption are both presented. (For interpretation of the references to color in this figure legend, the reader is referred to the web version of this article.)

Table 4
SSLs derived from the inverse mode of the integrated modeling framework for the Loam 2 soil for both the AFFF-impacted fire training and the biosolids-impacted agricultural sites. The SSLs for the three precipitation levels and with vs. without accounting for air–water interfacial (AWI) adsorption are presented.

	PFAS	Derived SSL (μg/kg)					
		30 cm precipitation		60 cm precipitation		120 cm precipitation	
		w/ AWI adsorption	w/o AWI adsorption	w/ AWI adsorption	w/o AWI adsorption	w/ AWI adsorption	w/o AWI adsorption
AFFF	PFPeA	2,165	1,962	569	538	153	150
	PFHxA	2,927	2,334	728	637	192	177
	PFHpA	11,767	6,395	2,504	1,701	564	459
	PFOA	176	36.2	30.3	9.55	5.28	2.55
	PFNA	16,963	820	2,623	210	373	54.1
	PFDA	19,072	2,348	2,756	590	435	149
	PFBS	2,290	2,085	602	571	162	157
	PFHxS	76.5	33.6	15.3	8.93	3.29	2.43
	PFOS	8,629	673	1,363	171	201	43.4
Biosolids	PFPeA	5.47	5.25	4.20	4.03	2.54	2.49
	PFHxA	6.89	6.21	5.18	4.79	3.15	2.93
	PFHpA	22.5	16.4	16.2	12.5	9.20	7.67
	PFOA	0.25	0.09	0.17	0.07	0.08	0.04
	PFNA	20.3	2.00	13.0	1.50	5.27	0.89
	PFDA	22.0	5.57	14.5	4.15	6.37	2.43
	PFBS	5.82	5.53	4.43	4.29	2.68	2.61
	PFHxS	0.13	0.09	0.10	0.07	0.05	0.04
	PFOS	10.6	1.61	6.87	1.21	2.88	0.71

is not exceeded initially, we still derive an SSL as a reference. We do so by incrementally adding mass to the input soil profile until the peak concentration in the receptor well is just below the MCL. The upper bound of the end soil concentration may be considered as an SSL for the PFAS at that specific site condition.

We begin by looking at some illustrative examples of the derived SSLs for three PFAS (PFHxS, PFOA, and PFOS) for the case of Loam 2 soil at 30 cm precipitation at the AFFF-impacted site (Fig. 8). The MCL presented in Table 1 are used to derive the SSLs. The initial simulated PFAS concentration at the groundwater receptor well (above the MCL) and that after removing PFAS mass in the soil (below the MCL) are both presented. The derived SSL increases with chain length, with the SSL for PFOS being much greater than that for PFOA and PFHxS. To illustrate how air–water interfacial adsorption affects the SSLs, we also present the derived SSLs where the air–water interfacial adsorption is turned off in the analytical vadose-zone transport model. The results indicate that not accounting for air–water interfacial adsorption leads to substantially smaller SSLs. The SSLs decrease by a factor of approximately 13, 5, and 2 for PFOS, PFOA, and PFHxS, respectively.

Similar trends for the derived SSLs are observed for the other PFAS for the same case of Loam 2 soil under different precipitation levels at the AFFF-impacted site (Table 4). For the same MCL, PFAS with

Table 5
Comparisons of the SSLs derived from the iterative inverse mode of the integrated modeling framework versus those derived using the vadose-zone attenuation factor ("VZ-AF") approach described in Eq. (4). The case of the Loam 2 soil at the precipitation level of 60 cm is used as an example for both the AFFF-impacted fire training and Biosolids-impacted agricultural sites. The two approaches give almost identical SSLs (within 0.5% difference).

PFAS	AFFF site			Biosolids site		
	$SSL_{Iterative}$ (μg/kg)	SSL_{VZ-AF} (μg/kg)	Difference (–)	$SSL_{Iterative}$ (μg/kg)	SSL_{VZ-AF} (μg/kg)	Difference (–)
PFPeA	569.0	569.8	0.1%	4.20	4.22	0.4%
PFHxA	728.0	728.8	0.1%	5.18	5.20	0.3%
PFHpA	2503.6	2506.9	0.1%	16.24	16.30	0.4%
PFOA	30.3	30.4	0.2%	0.17	0.17	0.1%
PFNA	2623.4	2631.6	0.3%	13.01	13.01	0.0%
PFDA	2756.4	2765.5	0.3%	14.46	14.50	0.3%
PFBS	601.9	602.6	0.1%	4.43	4.43	0.1%
PFHxS	15.3	15.4	0.3%	0.10	0.10	0.5%
PFOS	1363.1	1364.5	0.1%	6.87	6.89	0.2%

higher attenuation factors have a greater derived SSL, confirming that accurately representing the attenuation processes in the vadose zone is critical for reducing uncertainties in the derived SSLs. There are two additional observations. First, greater precipitation levels (hence greater net infiltration rates) significantly reduce the SSLs for all PFAS. This is true both with and without accounting for air–water interfacial adsorption, but the reduction is greater when air–water interfacial adsorption is included, especially for the more interfacially-active longer-chain PFAS. For example, the SSL for PFOS decreases from 8629 ug/kg to 201 ug/kg (with air–water interfacial adsorption) and 673 ug/kg to 43.4 ug/kg (without air–water interfacial adsorption) respectively, when the precipitation level increases from 30 cm to 120 cm. Second, the impact of precipitation level increases for longer-chain PFAS as expected. This is because greater net infiltration rates lead to greater water saturation that subsequently reduces the air–water interfacial area and hence the overall retention, especially for the more interfacially-active longer-chain PFAS. For instance, the SSLs for PFDA and PFOS (the two longest-chain PFAS) decrease by a factor of 44 and 43, respectively, when the precipitation level increases from 30 cm to 120 cm. Conversely, the SSLs for PFPeA and PFBS (the two shortest-chain PFAS) are both reduced by a factor of 14.

We have also derived the SSLs for the biosolids-impacted site (Table 4). The biosolids-impacted site shares the same general trend as those observed in the AFFF-impacted site, but the derived SSLs are much smaller—by a factor between 60 to 868 depending on the specific PFAS and precipitation level. A closer inspection reveals that this is caused by two factors. The first is the significantly smaller dilution factors in groundwater at the biosolids-impacted site resulting from the much greater site dimension based on Eq. (1) as discussed in Section 4.1. The other reason is that the biosolids-impacted site has additional net infiltration from irrigation (9.144 cm per year), which enhances PFAS leaching in the vadose zone (Eq. (1)).

Regarding the dependence of the groundwater dilution factor on the dimension of the contaminated site, the dilution factor approach (USEPA, 1996) used in the present study assumes that the receptor well is at the edge of the contaminated source zone and there is no dilution from recharge downgradient of the site. While a greater site dimension W increases the thickness of the groundwater mixing zone (δ_{gw}), δ_{gw} cannot exceed the thickness of the saturated zone (b_{sat}). Because the dilution factor scales inversely with W (Eq. (1)), the dilution factor can decrease substantially as the site dimension (W) becomes large, which is the case of the biosolids-impacted site. Note that the thickness of the saturated zone is set to b_{sat} = 3.05 m in the present study. For sites with a greater thickness of the saturated zone, the biosolids-impacted sites may have greater dilution factors, which may lead to greater SSLs. See Tables S1–S5 in the SI for derived SSLs for the other 5 soil types included in the present study.

In addition to deriving the SSLs from the iterative inverse mode of the integrated modeling framework as described above, we present another more direct approach by employing the vadose-zone attenuation factor computed in Section 4.1. Given the vadose-zone attenuation factor (AF_{vz}) for each specific site condition and PFAS, we can derive the SSL following the revised DAF approach proposed by Brusseau and Guo (2023) as

$$SSL_{VZ\text{-}AF} = C_{gw} \times AF_{vz} \times DF \times [K_d + (K_{aw}A_{aw} + \theta_w)\frac{1}{\rho_b}], \quad (4)$$

where, as presented in Section 4.1, the vadose-zone attenuation factor (AF_{vz}) is defined as the ratio between the maximum porewater concentration of PFAS in the vadose zone and the maximum PFAS concentration in the leachate discharged to groundwater, which represents the PFAS-specific attenuation processes in the vadose zone. C_{gw} (μg/L) is an acceptable concentration in a groundwater receptor well (the assumed MCLs in Table 1 are used in the present study), DF (–) is the dilution factor in groundwater computed from Eq. (1), K_d is the solid-phase adsorption coefficient (cm^3/g), K_{aw} is the air–water interfacial adsorption coefficient (cm^3/cm^2), A_{aw} is the specific air–water interfacial area (cm^2/cm^3), θ_w is volumetric water content (–), and ρ_b is the soil bulk density (g/cm^3). The terms in the brackets serve to convert the porewater concentration to the soil concentration based on equilibrium mass partitioning between the porewater, solid surface, and air–water interfaces (Brusseau and Guo, 2023). We refer to the SSL computed in Eq. (4) as $SSL_{VZ\text{-}AF}$ to differentiate it from the SSL derived from the iterative inverse mode, $SSL_{Iterative}$.

We compute $SSL_{VZ\text{-}AF}$ and compare it to $SSL_{Iterative}$ derived from the iterative inverse mode of the integrated modeling framework (Table 5). While the SSLs are derived from two different approaches, they are almost identical with less than 0.5% difference across all PFAS and site conditions. The good agreement between the SSLs derived from the two approaches indicates that the vadose-zone attenuation factor effectively represents the attenuation processes of PFAS in the vadose zone and may be used in a vadose-zone attenuation and groundwater dilution factor approach to derive SSLs following the USEPA's DAF approach. Because the $SSL_{VZ\text{-}AF}$ and $SSL_{Iterative}$ are identical, we use the $SSL_{VZ\text{-}AF}$ and refer to it as the $SSL_{current\ study}$ hereafter. It is worth noting that the iterative inverse approach does have an advantage over the vadose-zone attenuation approach in that it can derive an SSL profile as a function of depth rather than a single SSL value. This additional information may be useful for determining remedial objectives and strategies.

5. Comparison with the USEPA SSL derivations

We compare our new SSL approach (Eq. (4)) presented in Section 4.2 to the earlier USEPA standard SSL derivation and that recently revised by Brusseau and Guo (2023). We begin with the standard USEPA approach described in USEPA (1996)

$$SSL = C_{gw} \times DAF \times [K_d + (\theta_w + \theta_a H)\frac{1}{\rho_b}], \quad (5)$$

where DAF is a dilution and attenuation factor (–), θ_a is volumetric air content (–), and H represents the Henry's Law constant (–). The other variables are the same as those defined in Eq. (4). The terms in

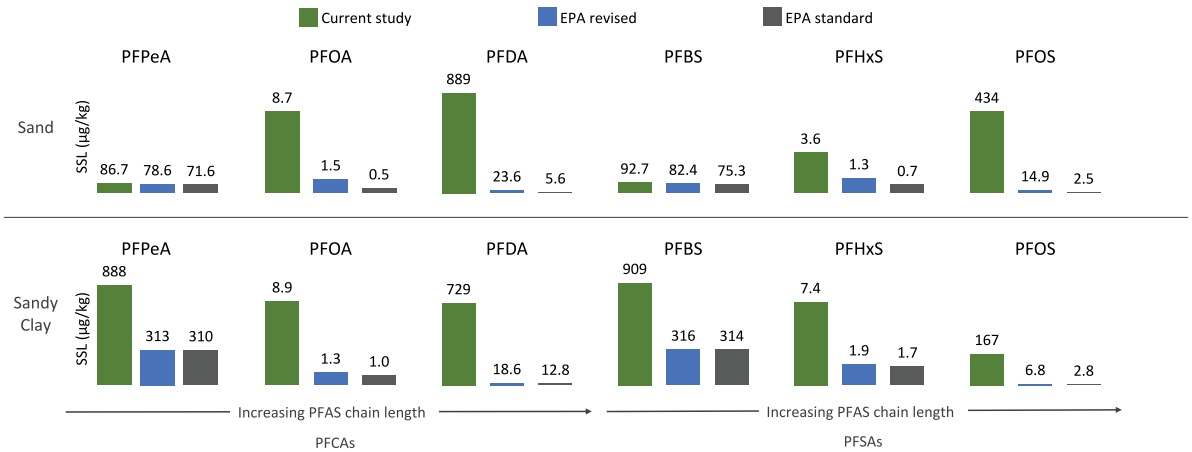

Fig. 9. Comparisons of the SSLs derived from our current study (Eq. (4)), Brusseau and Guo (2023)'s USEPA revised approach, and the USEPA standard approach. The Sand and Sandy Clay soils at the precipitation level of 60 cm for the AFFF-impacted fire training site are presented as examples.

the brackets convert the porewater concentration to the soil concentration based on equilibrium mass partitioning between the porewater, solid surface, and the air phase. The DAF in Eq. (5) considers only contaminant dilution in groundwater and thus does not represent any attenuation in the vadose zone. For illustrative purposes, we neglect the partitioning of contaminants in the air phase in the present study when comparing the different SSL derivation approaches. Furthermore, we use DF to replace DAF to reflect that it only accounts for dilution in groundwater. In the present study, DF is computed from Eq. (1). We then obtain the following simplified version of the USEPA standard SSL approach

$$\mathrm{SSL}_{\mathrm{EPA\ standard}} = C_{gw} \times DF \times [K_d + \frac{\theta_w}{\rho_b}]. \tag{6}$$

Brusseau and Guo (2023) revised the USEPA SSL approach to include the mass partitioning of PFAS at the air–water interfaces when converting the porewater concentration to the soil concentration. In the simplified version, the revised SSL approach has the following form

$$\mathrm{SSL}_{\mathrm{EPA\ revised}} = C_{gw} \times DF \times [K_d + (K_{aw} a_{aw} + \theta_w)\frac{1}{\rho_b}]. \tag{7}$$

As discussed in Section 1, the revised SSL approach by Brusseau and Guo (2023) (Eq. (7)) also does not represent any attenuation in the vadose zone, such as that caused by the retention of PFAS at air–water or solid–water interfaces during leaching. Inspection of the three SSL approaches (Eqs. (4)–(7)) reveals that our new SSL approach (Eq. (4)) is the only one that accounts for the attenuation of PFAS in the vadose zone via the vadose-zone attenuation factor AF_{vz}.

To illustrate the impact of including vadose-zone attenuation on the derived SSLs, we present in Fig. 9 the SSLs derived from our current study (Eq. (4)), Brusseau and Guo (2023)'s USEPA revised approach (Eq. (7)), and the USEPA standard approach (Eq. (6)). The Sand and Sandy Clay soils at the precipitation level of 60 cm for the AFFF-impacted fire training site are presented as examples. Additional comparisons for other soils are presented in the SI. The comparisons show that while the $\mathrm{SSL}_{\mathrm{EPA\ revised}}$ are greater than those by $\mathrm{SSL}_{\mathrm{EPA\ standard}}$ consistent with that reported in Brusseau and Guo (2023), the SSLs from our current study are uniformly greater than those by both previous approaches. Relatively small differences are observed for the shorter-chain PFAS among the three SSLs, but the difference increases greatly for longer-chain PFAS for both PFCAs and PFSAs. For the two shortest-chain PFPeA and PFBS, the three SSLs are comparable for Sand, and the $\mathrm{SSL}_{\mathrm{Current\ study}}$ is approximately 2.5 and 3 times greater than the other two for the Sandy Clay soil. Conversely, the $\mathrm{SSL}_{\mathrm{Current\ study}}$ of the longest-chain PFDA and PFOS are over 38 and 29 times greater than the $\mathrm{SSL}_{\mathrm{EPA\ revised}}$ and 159 and 174 times greater than the $\mathrm{SSL}_{\mathrm{EPA\ standard}}$ for the Sand, respectively. Similar trends of the differences are observed for the Sandy Clay and other soils (see SI), which is consistent with the attenuation factors presented in Fig. 4. The ratios between the SSLs derived from the three SSL approaches decrease under greater precipitation levels (i.e., greater net infiltration rates), indicating as discussed previously that net recharge is a critical parameter to determine when estimating site-specific SSLs. It is interesting that the $\mathrm{SSL}_{\mathrm{Current\ study}}$ for the longer-chain PFAS is still one order of magnitude or greater than the $\mathrm{SSL}_{\mathrm{EPA\ revised}}$ and $\mathrm{SSL}_{\mathrm{EPA\ standard}}$ even for the precipitation level of 120 cm (see SI Figure S13). Because the solid–water and air–water interfacial adsorption are primary factors affecting PFAS attenuation in the vadose zone, we have examined the sensitivity of the derived SSLs to both the solid–water and air–water interfacial adsorption coefficients (see figures S14 & S15 in the SI). The results suggest that the uncertainty in these two parameters linearly propagates to the derived SSLs and the relative importance of the uncertainty in the solid–water and air–water interfacial adsorption is a function of the soil type and PFAS.

The above results and analyses suggest that it is critical to include the attenuation of PFAS in the vadose zone for accurately estimating site-specific SSLs given an acceptable concentration in a groundwater receptor well at the site, especially for the more interfacially-active longer-chain PFAS. While not accounting for vadose-zone attenuation has a limited impact on the SSLs for the shorter-chain PFAS, it can lead to 1 to 2 orders of magnitude lower SSLs for the longer-chain PFAS.

6. Conclusion

We have developed a new integrated modeling framework that combines an analytical vadose-zone transport model that includes PFAS-specific retention processes (Guo et al., 2022) with a relatively simple approach that accounts for the dilution of PFAS by mixing in groundwater (USEPA, 1996). We have illustrated with specific examples that the analytical modeling framework can be used in a forward mode to characterize the risk of PFAS contamination in a groundwater receptor well near the contaminated site as well as in inverse modes to derive SSLs given an acceptable concentration in a groundwater receptor well. Furthermore, we have demonstrated that the analytical vadose-zone transport model can be used to obtain an effective attenuation factor for PFAS leaching in the vadose zone. The computed vadose-zone attenuation factor for specific site conditions can be directly used to derive SSLs following the general framework of the USEPA's DAF approach.

The example applications for two model PFAS-contaminated sites (AFFF-impacted fire training area site and biosolids-impacted agricultural site) and the analyses over a wide range of site conditions suggest that adsorption at the air–water interfaces is a primary factor

that needs to be considered when characterizing PFAS contamination risks in groundwater receptor wells near PFAS-contaminated sites. Not accounting for retention due to adsorption at the air–water interfaces, as well as the solid–water interfaces, can lead to significantly greater peak simulated concentrations (up to an order of magnitude under certain conditions) in the groundwater receptor well, especially for the more interfacially-active longer-chain PFAS. Accordingly, not accounting for the attenuation of PFAS in the vadose zone will also lead to significantly underestimated SSLs at PFAS-contaminated sites. While the SSLs derived by our integrated modeling framework are comparable to those by the USEPA SSL approaches for the shortest-chain PFAS, the SSLs are 1 to 2 orders of magnitude greater than the SSLs derived from the USEPA standard SSL approach for longer-chain PFAS under most of the site conditions investigated in the present study. In addition to characterizing groundwater contamination risks and determining SSLs, it is anticipated that the analytical modeling framework can also be used for more general site characterization and remedial selection/assessment efforts, which will lead to an improved capacity to determine, manage, and mitigate risks associated with PFAS-contaminated sites.

CRediT authorship contribution statement

Jacob Smith: Methodology, Investigation, Software, Data curation, Formal analysis, Visualization, Writing – original draft. **Mark L. Brusseau:** Methodology, Funding acquisition, Writing – review & editing. **Bo Guo:** Conceptualization, Methodology, Investigation, Software, Data curation, Formal analysis, Visualization, Funding acquisition, Project administration, Supervision, Writing – review & editing.

Declaration of competing interest

The authors declare that they have no known competing financial interests or personal relationships that could have appeared to influence the work reported in this paper.

Data availability

All of the data used in the present study are provided in the manuscript or in the supporting information.

Acknowledgments

This work was in part supported by the Environmental Security Technology Certification Program (ESTCP Project ER21-5041). The integrated analytical modeling framework presented in the paper is being implemented in Excel as a user-friendly tool and will be released to the public free of charge as part of the PFAS-LEACH decision support platform at the completion of the ESTCP Project ER21-5041. We thank the reviewers for their supportive and constructive comments.

Appendix A. Supplementary data

Supplementary material related to this article can be found online at https://doi.org/10.1016/j.watres.2024.121236.

References

Adamson, D.T., Nickerson, A., Kulkarni, P.R., Higgins, C.P., Popovic, J., Field, J., Rodowa, A., Newell, C., DeBlanc, P., Kornuc, J.J., 2020. Mass-based, field-scale demonstration of PFAS retention within AFFF-Associated Source Areas. Environ. Sci. Technol. 54 (24), 15768–15777.

Anderson, R.H., 2021. The case for direct measures of soil-to-groundwater contaminant mass discharge at AFFF-impacted sites. Environ. Sci. Technol. 55 (10), 6580–6583.

Anderson, R.H., Adamson, D.T., Stroo, H.F., 2019. Partitioning of poly-and perfluoroalkyl substances from soil to groundwater within aqueous film-forming foam source zones. J. Contam. Hydrol. 220, 59–65.

Anderson, R.H., Feild, J.B., Dieffenbach-Carle, H., Elsharnouby, O., Krebs, R.K., 2022. Assessment of PFAS in collocated soil and porewater samples at an AFFF-impacted source zone: Field-scale validation of suction lysimeters. Chemosphere 308, 136247.

Bradford, S.A., Leij, F.J., 1997. Estimating interfacial areas for multi-fluid soil systems. J. Contam. Hydrol. 27 (1–2), 83–105.

Brusseau, M.L., 2018. Assessing the potential contributions of additional retention processes to PFAS retardation in the subsurface. Sci. Total Environ. 613, 176–185.

Brusseau, M.L., 2023. Determining air–water interfacial areas for the retention and transport of PFAS and other interfacially active solutes in unsaturated porous media. Sci. Total Environ. 163730.

Brusseau, M.L., Anderson, R.H., Guo, B., 2020. PFAS concentrations in soils: Background levels versus contaminated sites. Sci. Total Environ. 740, 140017.

Brusseau, M.L., Guo, B., 2023. Revising the EPA dilution-attenuation soil screening model for PFAS. J. Hazard. Mater. Lett. 4, 100077.

Brusseau, M.L., Khan, N., Wang, Y., Yan, N., van Glubt, S., Carroll, K.C., 2019. Nonideal transport and extended elution tailing of PFOS in soil. Environ. Sci. Technol..

Buck, R.C., Franklin, J., Berger, U., Conder, J.M., Cousins, I.T., De Voogt, P., Jensen, A.A., Kannan, K., Mabury, S.A., van Leeuwen, S.P., 2011. Perfluoroalkyl and polyfluoroalkyl substances in the environment: Terminology, classification, and origins. Integr. Environ. Assess. Manag. 7 (4), 513–541.

Cáñez, T.T., Guo, B., McIntosh, J.C., Brusseau, M.L., 2021. Perfluoroalkyl and polyfluoroalkyl substances (PFAS) in groundwater at a reclaimed water recharge facility. Sci. Total Environ. 147906.

Connor, J., Bowers, R., Paquette, S., Newell, C., 1997. Soil Attenuation Model for Derivation of Risk-Based Soil Remediation Standards. Groundwater Services Inc., Houston, Texas, pp. 1–34.

Costanza, J., Arshadi, M., Abriola, L.M., Pennell, K.D., 2019. Accumulation of PFOA and PFOS at the air–water interface. Environ. Sci. Technol. Lett. 6 (8), 487–491.

Dauchy, X., Boiteux, V., Colin, A., Hémard, J., Bach, C., Rosin, C., Munoz, J.-F., 2019. Deep seepage of per- and polyfluoroalkyl substances through the soil of a firefighter training site and subsequent groundwater contamination. Chemosphere 214, 729–737.

FAA, F.A.A., 2010. Advisory circular: Aircraft Rescue and Fire Fighting (ARFF) training facilities. AC No:150/5220-17B, Federal US Department of Transportation.

Gnesda, W.R., Draxler, E.F., Tinjum, J., Zahasky, C., 2022. Adsorption of PFAAs in the vadose zone and implications for long-term groundwater contamination. Environ. Sci. Technol. 56 (23), 16748–16758.

Guo, B., Zeng, J., Brusseau, M.L., 2020. A mathematical model for the release, transport, and retention of per-and polyfluoroalkyl substances (PFAS) in the vadose zone. Water Resour. Res. 56 (2), e2019WR026667.

Guo, B., Zeng, J., Brusseau, M.L., Zhang, Y., 2022. A screening model for quantifying PFAS leaching in the vadose zone and mass discharge to groundwater. Adv. Water Resour. 160, 104102.

Healy, R.W., 2010. Estimating Groundwater Recharge. Cambridge University Press.

Høisæter, Å., Pfaff, A., Breedveld, G.D., 2019. Leaching and transport of PFAS from aqueous film-forming foam (AFFF) in the unsaturated soil at a firefighting training facility under cold climatic conditions. J. Contam. Hydrol. 222, 112–122.

ITRC, 2019. History and Use of Per- and Polyfluoroalkyl Substances (PFAS) Found in the Environment. Technical Report, The Interstate Technology and Regulatory Council (ITRC).

Jiang, H., Guo, B., Brusseau, M.L., 2020. Pore-scale modeling of fluid-fluid interfacial area in variably saturated porous media containing microscale surface roughness. Water Resour. Res. 56 (1), e2019WR025876.

Leverett, M., 1941. Capillary behavior in porous solids. Trans. AIME 142 (01), 152–169.

Lyu, Y., Brusseau, M.L., Chen, W., Yan, N., Fu, X., Lin, X., 2018. Adsorption of PFOA at the air–water interface during transport in unsaturated porous media. Environ. Sci. Technol. 52 (14), 7745–7753.

Moodie, D., Coggan, T., Berry, K., Kolobaric, A., Fernandes, M., Lee, E., Reichman, S., Nugegoda, D., Clarke, B.O., 2021. Legacy and emerging per-and polyfluoroalkyl substances (PFASs) in Australian biosolids. Chemosphere 270, 129143.

Morrow, N.R., 1970. Physics and thermodynamics of capillary action in porous media. Ind. Eng. Chem. 62 (6), 32–56.

Newell, C.J., Stockwell, E.B., Alanis, J., Adamson, D.T., Walker, K.L., Anderson, R.H., 2023. Determining groundwater recharge for quantifying PFAS mass discharge from unsaturated source zones. Vadose Zone J. e20262.

Nguyen, T.M.H., Braunig, J., Thompson, K., Thompson, J., Kabiri, S., Navarro, D.A., Kookana, R.S., Grimison, C., Barnes, C.M., Higgins, C.P., 2020. Influences of chemical properties, soil properties, and solution pH on soil–water partitioning coefficients of per- and polyfluoroalkyl substances (PFASs). Environ. Sci. Technol. 54 (24), 15883–15892.

Pepper, I.L., Brusseau, M.L., Prevatt, F.J., Escobar, B.A., 2021. Incidence of PFAS in soil following long-term application of class B biosolids. Sci. Total Environ. 793, 148449.

Quinnan, J., Rossi, M., Curry, P., Lupo, M., Miller, M., Korb, H., Orth, C., Hasbrouck, K., 2021. Application of PFAS-mobile lab to support adaptive characterization and flux-based conceptual site models at AFFF releases. Remediat. J. 31 (3), 7–26.

Rovero, M., Cutt, D., Griffiths, R., Filipowicz, U., Mishkin, K., White, B., Goodrow, S., Wilkin, R.T., 2021. Limitations of current approaches for predicting groundwater vulnerability from PFAS contamination in the vadose zone. Groundw. Monit. Remediat. 41 (4), 62–75.

Scanlon, B.R., Healy, R.W., Cook, P.G., 2002. Choosing appropriate techniques for quantifying groundwater recharge. Hydrogeol. J. 10, 18–39.

Schaefer, C.E., Culina, V., Nguyen, D., Field, J., 2019a. Uptake of poly- and perfluoroalkyl substances at the air–water interface. Environ. Sci. Technol. 53 (21), 12442–12448.

Schaefer, C.E., Drennan, D.M., Tran, D.N., Garcia, R., Christie, E., Higgins, C.P., Field, J.A., 2019b. Measurement of aqueous diffusivities for perfluoroalkyl acids. J. Environ. Eng. 145 (11), 06019006.

Schaefer, C.E., Lavorgna, G.M., Lippincott, D.R., Nguyen, D., Christie, E., Shea, S., O'Hare, S., Lemes, M.C., Higgins, C.P., Field, J., 2022. A field study to assess the role of air–water interfacial sorption on PFAS leaching in an AFFF source area. J. Contam. Hydrol. 248, 104001.

Schaefer, C.E., Lavorgna, G.M., Lippincott, D.R., Nguyen, D., Schaum, A., Higgins, C.P., Field, J., 2023. Leaching of perfluoroalkyl acids during unsaturated zone flushing at a field site impacted with aqueous film forming foam. Environ. Sci. Technol. 57 (5), 1940–1948.

Schaefer, C.E., Nguyen, D., Christie, E., Shea, S., Higgins, C.P., Field, J.A., 2021. Desorption of poly- and perfluoroalkyl substances from soil historically impacted with aqueous film-forming foam. J. Environ. Eng. 147 (2), 06020006.

Sepulvado, J.G., Blaine, A.C., Hundal, L.S., Higgins, C.P., 2011. Occurrence and fate of perfluorochemicals in soil following the land application of municipal biosolids. Environ. Sci. Technol. 45 (19), 8106–8112.

Silva, J.A., Martin, W.A., Johnson, J.L., McCray, J.E., 2019. Evaluating air–water and NAPL-water interfacial adsorption and retention of perfluorocarboxylic acids within the vadose zone. J. Contam. Hydrol. 223, 103472.

Silva, J.A., Martin, W.A., McCray, J.E., 2021. Air–water interfacial adsorption coefficients for PFAS when present as a multi-component mixture. J. Contam. Hydrol. 236, 103731.

Silva, J.A.K., Simunek, J., McCray, J.E., 2020. A modified HYDRUS model for simulating PFAS transport in the vadose zone. Water 12 (10), 2758.

Silva, J.A., Šimůnek, J., McCray, J.E., 2022. Comparison of methods to estimate air–water interfacial areas for evaluating PFAS transport in the vadose zone. J. Contam. Hydrol. 247, 103984.

Stephens, D., Johnson, P., Havlena, J., 1996. Estimation of infiltration and recharge for environmental site assessment. API Publ. 4643, 143.

USDA, 2020. Arizona Agricultural Statistics 2020. Technical Report, USDA, Arizona Department of Agriculture.

USDA-NASS, 2019. USDA-NASS, 2019. Part 1. 2017 Census of Agriculture, 2018 Irrigation and Water Management Survey. AC-17-SS-1. Special Studies, vol. 3. Table 4. Technical Report, United States Department of Agriculture National Agricultural Statistics Service, Washington, DC.

USEPA, 1996. Soil Screening Guidance: User's Guide. Office of Solid Waste and Emergency Response, EPA.

USEPA, 2000. Biosolids Technology Fact Sheet: Land Application of Biosolids. USEPA Washington, DC, USA.

USEPA, 2023a. Proposed PFAS National Primary Drinking Water Regulation. Technical Report, United States Environmental Protection Agency.

USEPA, 2023b. Regional Screening Levels (RSLs) - User's Guide. USEPA Washington, DC, USA.

Venkatesan, A.K., Halden, R.U., 2013. National inventory of perfluoroalkyl substances in archived US biosolids from the 2001 EPA National Sewage Sludge Survey. J. Hazard. Mater. 252, 413–418.

Wallis, I., Hutson, J., Davis, G., Kookana, R., Rayner, J., Prommer, H., 2022. Model-based identification of vadose zone controls on PFAS mobility under semi-arid climate conditions. Water Res. 225, 119096.

Weber, A.K., Barber, L.B., LeBlanc, D.R., Sunderland, E.M., Vecitis, C.D., 2017. Geochemical and hydrologic factors controlling subsurface transport of poly-and perfluoroalkyl substances, Cape Cod, Massachusetts. Environ. Sci. Technol. 51 (8), 4269–4279.

Xiao, F., Simcik, M.F., Halbach, T.R., Gulliver, J.S., 2015. Perfluorooctane sulfonate (PFOS) and perfluorooctanoate (PFOA) in soils and groundwater of a US metropolitan area: Migration and implications for human exposure. Water Res. 72, 64–74.

Xu, M., Eckstein, Y., 1995. Use of weighted least-squares method in evaluation of the relationship between dispersivity and field scale. Groundwater 33 (6), 905–908.

Zeng, J., Brusseau, M.L., Guo, B., 2021. Model validation and analyses of parameter sensitivity and uncertainty for modeling long-term retention and leaching of PFAS in the vadose zone. J. Hydrol. 127172.

Zeng, J., Guo, B., 2021. Multidimensional simulation of PFAS transport and leaching in the vadose zone: Impact of surfactant-induced flow and subsurface heterogeneities. Adv. Water Resour. 155, 104015.

Zeng, J., Guo, B., 2023. Reduced accessible air–water interfacial area accelerates PFAS leaching in heterogeneous vadose zones. Geophys. Res. Lett. 50 (8), e2022GL102655.

Zhang, Y., Schaap, M.G., 2017. Weighted recalibration of the Rosetta pedotransfer model with improved estimates of hydraulic parameter distributions and summary statistics (Rosetta3). J. Hydrol. 547, 39–53.